

## INFORMATION TO USERS

This manuscript has been reproduced from the microfilm master. UMI films the text directly from the original or copy submitted. Thus, some thesis and dissertation copies are in typewriter face, while others may be from any type of computer printer.

**The quality of this reproduction is dependent upon the quality of the copy submitted.** Broken or indistinct print, colored or poor quality illustrations and photographs, print bleedthrough, substandard margins, and improper alignment can adversely affect reproduction.

In the unlikely event that the author did not send UMI a complete manuscript and there are missing pages, these will be noted. Also, if unauthorized copyright material had to be removed, a note will indicate the deletion.

Oversize materials (e.g., maps, drawings, charts) are reproduced by sectioning the original, beginning at the upper left-hand corner and continuing from left to right in equal sections with small overlaps.

ProQuest Information and Learning  
300 North Zeeb Road, Ann Arbor, MI 48106-1346 USA  
800-521-0600

UMI<sup>®</sup>

PREVIEW

# ABSTRACT

In this dissertation, the method of moments technique for analyzing electromagnetic scattering from an arbitrarily shaped three-dimensional homogeneous chiral body is presented based on the combined field integral equations. The body is assumed to be illuminated by a plane wave. The surface equivalence principle is used to replace the body by equivalent electric and magnetic surface currents. By enforcing the continuity of the tangential components of the total electric and magnetic fields on the surface of the body, a set of coupled integral equations is obtained. The surface of the body is modeled using triangular patches. The triangular rooftop vector expansion functions are used for both equivalent surface currents. The coefficients of these expansion functions are obtained using the method of moments. The mixed potential formulation for a chiral medium is developed and used to obtain explicit expressions for the electric and magnetic fields produced by surface currents. Numerical results for bistatic radar cross sections, the internal field, and the equivalent surface currents along the perimeter of a cross section of the chiral body are presented for three chiral scatterers—a sphere, a finite circular cylinder, and a cube.

Numerical results for a sphere are in excellent agreement with the exact ones found by the eigenfunction solution. An analysis of convergence and a possibility of using the right- and left-handed equivalent surface currents as independent unknowns are briefly discussed. Finally, a sufficient condition for obtaining zero cross-polarized backscattering cross section is presented.

In an appendix, the exact solutions for a resonant frequency and a  $Q$  factor of a chiral sphere are derived.

PREVIEW

# **ELECTROMAGNETIC SCATTERING FROM AN ARBITRARILY SHAPED THREE-DIMENSIONAL CHIRAL BODY**

by

**DENCHAI WORASAWATE**  
B.S. Kasetsart University, 1995  
M.S. Syracuse University, 2000

**DISSERTATION**

**Submitted in partial fulfillment of the requirements for the degree of Doctor of  
Philosophy in Electrical Engineering in the Graduate School of Syracuse University**

**August 2002**

Approved E. Arvas  
Professor Ercument Arvas

Date 7/15/2002

**UMI Number: 3065208**

**Copyright 2002 by  
Worasawate, Denchai**

**All rights reserved.**

**UMI<sup>®</sup>**

---

**UMI Microform 3065208**

**Copyright 2002 by ProQuest Information and Learning Company.  
All rights reserved. This microform edition is protected against  
unauthorized copying under Title 17, United States Code.**

---

**ProQuest Information and Learning Company  
300 North Zeeb Road  
P.O. Box 1346  
Ann Arbor, MI 48106-1346**

**Copyright 2002 Denchai Worasawate**

**All rights Reserved**

PREVIEW

**The Graduate School  
Syracuse University**

**We, the members of the Oral Examination Committee,  
hereby register our concurrence that**

**Denchai Worasawate**

**satisfactorily defended his dissertation on**

**Wednesday, July 10, 2002**

**Examiners:**

**Philipp Kornrieck**

  
(Please sign)

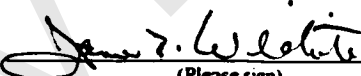
**Jay Lee**

  
(Please sign)

**Joseph Mautz**

  
(Please sign)

**James Willhite**

  
(Please sign)

  
(Please sign)

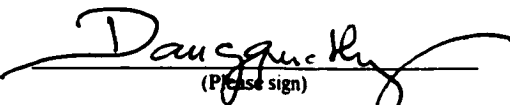
**Advisor:**

**Ercument Arvas**

  
(Please sign)

**Oral Examination Chair:**

**Thong Dang**

  
(Please sign)



# CONTENTS

<b>List of Figures</b>	.....	vii
<b>List of Tables</b>	.....	xv
<b>Acknowledgments</b>	.....	xvi
<b>Chapter 1</b>	<b>Introduction</b> .....	1
	1.1 Chiral Medium .....	1
	1.2 Constitutive Relations .....	3
	1.3 Motivation .....	5
	1.4 Contribution of This Dissertation .....	6
<b>Chapter 2</b>	<b>The Field of Sources in an Unbounded Chiral Medium</b> .	7
<b>Chapter 3</b>	<b>Electromagnetic Scattering from an Arbitrarily Shaped Three-Dimensional Homogeneous Chiral Body</b> .....	16
	3.1 Integral Equations .....	16
	3.2 Application of the Method of Moments .....	26
	3.3 Computation of the Elements of the Matrices .....	36
	3.4 Internal Field .....	40
	3.5 Radar Cross Section of a Chiral Body .....	41
<b>Chapter 4</b>	<b>Numerical Results and Discussion</b> .....	44
	4.1 Numerical Results for a Chiral Sphere .....	46
	4.2 Numerical Results for a Finite Circular Chiral Cylinder ....	68
	4.3 Numerical Results for a Chiral Cube .....	82
	4.4 Cross-Polarized Backscattering Cross Section .....	102
<b>Chapter 5</b>	<b>Conclusion</b> .....	110

<b>Appendix A</b>	<b>The Exact Solution for Electromagnetic Scattering and Resonance Problems Involving a Chiral Sphere . . . . .</b>	<b>113</b>
A.1	The Spherical Solutions for the Electromagnetic Field in a Chiral Medium . . . . .	113
A.2	Electromagnetic Scattering From a Chiral Sphere . . . . .	121
A.3	Electromagnetic Resonance of a Chiral Sphere . . . . .	137
A.4	The Solutions of the Characteristic Equations of a Dielectric Sphere when $\epsilon_r \rightarrow 1$ . . . . .	147
A.4.1	The Solutions of the TE Characteristic Equation when $\epsilon_r \rightarrow 1$ . . . . .	147
A.4.2	The Solutions of the TM Characteristic Equation when $\epsilon_r \rightarrow 1$ . . . . .	151
<b>Appendix B</b>	<b>Derivation of the Self-Term . . . . .</b>	<b>155</b>
<b>Appendix C</b>	<b>Evaluation of Integrals Appearing in the Mixed Potential Formulation . . . . .</b>	<b>160</b>
<b>Appendix D</b>	<b>Gaussian Quadrature Rules for the Triangle . . . . .</b>	<b>167</b>
<b>Appendix E</b>	<b>Derivation of the Curl of the Curl of the Radial Vector Potential . . . . .</b>	<b>172</b>
<b>Bibliography</b>	<b>. . . . .</b>	<b>174</b>
<b>VITA</b>	<b>. . . . .</b>	<b>179</b>

## List of Figures

Fig. 3.1.	The original problem. A plane wave illuminating an arbitrarily shaped three-dimensional isotropic homogeneous chiral body. . . . .	17
Fig. 3.2.	The external equivalence of the original problem of Fig. 3.1. . . . .	18
Fig. 3.3.	The internal equivalence of the original problem of Fig. 3.1. . . . .	18
Fig. 3.4.	A triangulated model of a sphere. . . . .	27
Fig. 3.5.	Triangle pair and geometrical parameters associated with the $n^{\text{th}}$ edge. . . . .	27
Fig. 4.1.	Geometries of scatterers considered in Sections 4.1–4.3. . . . .	45
Fig. 4.2.	$\sigma_{\theta\theta}$ of a chiral sphere, $k_0 a = 1.5$ , $\epsilon_r = 2$ , $\mu_r = 1$ , $\xi_r = 0.3$ . . . . .	50
Fig. 4.3.	$\sigma_{\phi\phi}$ of a chiral sphere, $k_0 a = 1.5$ , $\epsilon_r = 2$ , $\mu_r = 1$ , $\xi_r = 0.3$ . . . . .	50
Fig. 4.4.	Magnitude of $x$ -component of electric field internal to a chiral sphere along the $z$ -axis, $k_0 a = 1.5$ , $\epsilon_r = 2$ , $\mu_r = 1$ , $\xi_r = 0.3$ . . . . .	51
Fig. 4.5.	Phase of $x$ -component of electric field internal to a chiral sphere along the $z$ -axis, $k_0 a = 1.5$ , $\epsilon_r = 2$ , $\mu_r = 1$ , $\xi_r = 0.3$ . . . . .	51
Fig. 4.6.	Magnitude of $y$ -component of electric field internal to a chiral sphere along the $z$ -axis, $k_0 a = 1.5$ , $\epsilon_r = 2$ , $\mu_r = 1$ , $\xi_r = 0.3$ . . . . .	52
Fig. 4.7.	Phase of $y$ -component of electric field internal to a chiral sphere along the $z$ -axis, $k_0 a = 1.5$ , $\epsilon_r = 2$ , $\mu_r = 1$ , $\xi_r = 0.3$ . . . . .	52
Fig. 4.8.	Percent error of $ E_x $ along the $z$ -axis for a chiral sphere, $k_0 a = 1.5$ , $\epsilon_r = 2$ , $\mu_r = 1$ , $\xi_r = 0.0$ . . . . .	53
Fig. 4.9.	Percent error of $ E_x $ along the $z$ -axis for a chiral sphere, $k_0 a = 1.5$ , $\epsilon_r = 2$ , $\mu_r = 1$ , $\xi_r = 0.6$ . . . . .	53
Fig. 4.10.	Percent error of $ E_x $ along the $z$ -axis for a chiral sphere, $k_0 a = 1.5$ , $\epsilon_r = 2$ , $\mu_r = 1$ , $\xi_r = 0.7$ . . . . .	54

Fig. 4.11.	Percent error of $ E_x $ along the $z$ -axis for a chiral sphere, $k_o a = 1.5$ , $\epsilon_r = 2$ , $\mu_r = 1$ , $\xi_r = 0.8$ . . . . .	54
Fig. 4.12.	Percent error of $ E_x $ at $z = -0.805a$ for a chiral sphere, $k_o a = 1.5$ , $\epsilon_r = 2$ , $\mu_r = 1$ , $\xi_r = 0.0, 0.1, \dots, 0.9$ . . . . .	55
Fig. 4.13.	Percent error of $ E_x $ at $z = 0.795a$ for a chiral sphere, $k_o a = 1.5$ , $\epsilon_r = 2$ , $\mu_r = 1$ , $\xi_r = 0.0, 0.1, \dots, 0.9$ . Solid lines are computed by the approximating function. . . . .	55
Fig. 4.14.	Percent error of $\sigma_{\theta\theta}$ at $\theta = 0^\circ$ for a chiral sphere, $k_o a = 1.5$ , $\epsilon_r = 2$ , $\mu_r = 1$ , $\xi_r = 0.0, 0.1, \dots, 0.9$ . . . . .	56
Fig. 4.15.	Percent error of $\sigma_{\theta\theta}$ at $\theta = 180^\circ$ for a chiral sphere, $k_o a = 1.5$ , $\epsilon_r = 2$ , $\mu_r = 1$ , $\xi_r = 0.0, 0.1, \dots, 0.9$ . . . . .	56
Fig. 4.16.	$\sigma_{\theta\theta}$ of a chiral sphere, $k_o a = 1.5$ , $\epsilon_r = 2$ , $\mu_r = 1$ , $\xi_r = 0.0, 0.1, \dots, 0.9$ . . . . .	59
Fig. 4.17.	$\sigma_{\theta\theta}$ of a chiral sphere, $k_o a = 1.5$ , $\epsilon_r = 2$ , $\mu_r = 1$ , $\xi_r = 0.0, 0.1, \dots, 0.9$ . . . . .	60
Fig. 4.18.	$\sigma_{\theta\theta}$ of a chiral sphere, $k_o a = 1.5$ , $\epsilon_r = 2$ , $\mu_r = 1$ , at $\theta = 0^\circ, 45^\circ, 90^\circ, 135^\circ, 180^\circ$ . . . . .	61
Fig. 4.19.	$\sigma_{\theta\theta}$ of a chiral sphere, $k_o a = 1.5$ , $\epsilon_r = 2$ , $\mu_r = 1$ , at $\theta = 0^\circ, 45^\circ, 90^\circ, 135^\circ, 180^\circ$ . . . . .	61
Fig. 4.20.	Magnitude of $x$ -component of electric field internal to a chiral sphere along the $z$ -axis, $k_o a = 1.5$ , $\epsilon_r = 2$ , $\mu_r = 1$ , $\xi_r = 0.0, 0.3, 0.4, 0.5, 0.6, 0.7, 0.8$ , and $0.9$ . . . . .	62
Fig. 4.21.	Phase of $x$ -component of electric field internal to a chiral sphere along the $z$ -axis, $k_o a = 1.5$ , $\epsilon_r = 2$ , $\mu_r = 1$ , $\xi_r = 0.0, 0.3, 0.4, 0.5, 0.6, 0.7, 0.8$ , and $0.9$ . . . . .	62
Fig. 4.22.	Magnitude of $y$ -component of electric field internal to a chiral sphere along the $z$ -axis, $k_o a = 1.5$ , $\epsilon_r = 2$ , $\mu_r = 1$ , $\xi_r = 0.0, 0.1, \dots, 0.9$ . . . . .	63

Fig. 4.23.	Phase of $y$ -component of electric field internal to a chiral sphere along the $z$ -axis, $k_o a = 1.5$ , $\epsilon_r = 2$ , $\mu_r = 1$ , $\xi_r = 0.1, 0.2, \dots, 0.9$ . . .	63
Fig. 4.24.	Magnitude of $\phi$ -component of magnetic current in the $\phi = 0$ plane of a chiral sphere, $k_o a = 1.5$ , $\epsilon_r = 2$ , $\mu_r = 1$ , $\xi_r = 0.0, 0.4, 0.7, 0.8$ , and $0.9$ . . . . .	64
Fig. 4.25.	Phase of $\phi$ -component of magnetic current in the $\phi = 0$ plane of a chiral sphere, $k_o a = 1.5$ , $\epsilon_r = 2$ , $\mu_r = 1$ , $\xi_r = 0.0, 0.4, 0.7, 0.8$ , and $0.9$ . . . . .	64
Fig. 4.26.	Magnitude of $\theta$ -component of magnetic current in the $\phi = 0$ plane of a chiral sphere, $k_o a = 1.5$ , $\epsilon_r = 2$ , $\mu_r = 1$ , $\xi_r = 0.0, 0.4, 0.5, 0.6, 0.7, 0.8$ , and $0.9$ . . . . .	65
Fig. 4.27.	Phase of $\theta$ -component of magnetic current in the $\phi = 0$ plane of a chiral sphere, $k_o a = 1.5$ , $\epsilon_r = 2$ , $\mu_r = 1$ , $\xi_r = 0.4, 0.5, 0.6, 0.7, 0.8$ , and $0.9$ . . . . .	65
Fig. 4.28.	Magnitude of $\phi$ -component of electric current in the $\phi = 0$ plane of a chiral sphere, $k_o a = 1.5$ , $\epsilon_r = 2$ , $\mu_r = 1$ , $\xi_r = 0.0, 0.4, 0.7, 0.8$ , and $0.9$ . . . . .	66
Fig. 4.29.	Phase of $\phi$ -component of electric current in the $\phi = 0$ plane of a chiral sphere, $k_o a = 1.5$ , $\epsilon_r = 2$ , $\mu_r = 1$ , $\xi_r = 0.4, 0.7, 0.8$ , and $0.9$ . . . . .	66
Fig. 4.30.	Magnitude of $\theta$ -component of electric current in the $\phi = 0$ plane of a chiral sphere, $k_o a = 1.5$ , $\epsilon_r = 2$ , $\mu_r = 1$ , $\xi_r = 0.0, 0.4, 0.5, 0.6, 0.7, 0.8$ , and $0.9$ . . . . .	67
Fig. 4.31.	Phase of $\theta$ -component of electric current in the $\phi = 0$ plane of a chiral sphere, $k_o a = 1.5$ , $\epsilon_r = 2$ , $\mu_r = 1$ , $\xi_r = 0.0, 0.4, 0.5, 0.6, 0.7, 0.8$ , and $0.9$ . . . . .	67
Fig. 4.32.	Convergence of $ E_x/E^{\text{inc}} $ at $(x, y, z) = (0, 0, 0.4h)$ for a finite circular chiral cylinder, $k_o a = 1.5$ , $h = 0.35\lambda_o$ , $\epsilon_r = 2$ , $\mu_r = 1$ , $\xi_r = 0.0, 0.1, \dots, 0.9$ . . . . .	70

Fig. 4.33.	Estimated percent error of $ E_r $ at $(x, y, z) = (0, 0, 0.4h)$ for a finite circular chiral cylinder, $k_o a = 1.5$ , $h = 0.35\lambda_o$ , $\epsilon_r = 2$ , $\mu_r = 1$ , $\xi_r = 0.0, 0.1, \dots, 0.9$ . Solid lines are computed by the approximating function. ....	70
Fig. 4.34.	$\sigma_{\theta\theta}$ of a finite circular chiral cylinder, $k_o a = 1.5$ , $h = 0.35\lambda_o$ , $\epsilon_r = 2$ , $\mu_r = 1$ , $\xi_r = 0.0, 0.1, \dots, 0.9$ . ....	72
Fig. 4.35.	$\sigma_{\phi\phi}$ of a finite circular chiral cylinder, $k_o a = 1.5$ , $h = 0.35\lambda_o$ , $\epsilon_r = 2$ , $\mu_r = 1$ , $\xi_r = 0.0, 0.1, \dots, 0.9$ . ....	73
Fig. 4.36.	$\sigma_{\theta\theta}$ of a finite circular chiral cylinder, $k_o a = 1.5$ , $h = 0.35\lambda_o$ , $\epsilon_r = 2$ , $\mu_r = 1$ , at $\theta = 0^\circ, 45^\circ, 90^\circ, 135^\circ, 180^\circ$ ....	74
Fig. 4.37.	$\sigma_{\phi\phi}$ of a finite circular chiral cylinder, $k_o a = 1.5$ , $h = 0.35\lambda_o$ , $\epsilon_r = 2$ , $\mu_r = 1$ , at $\theta = 0^\circ, 45^\circ, 90^\circ, 135^\circ, 180^\circ$ ....	74
Fig. 4.38.	Magnitude of $x$ -component of electric field internal to a finite circular chiral cylinder along the $z$ -axis, $k_o a = 1.5$ , $h = 0.35\lambda_o$ , $\epsilon_r = 2$ , $\mu_r = 1$ , $\xi_r = 0.0, 0.3, 0.4, \dots, 0.9$ . ....	75
Fig. 4.39.	Phase of $x$ -component of electric field internal to a finite circular chiral cylinder along the $z$ -axis, $k_o a = 1.5$ , $h = 0.35\lambda_o$ , $\epsilon_r = 2$ , $\mu_r = 1$ , $\xi_r = 0.0, 0.3, 0.4, \dots, 0.9$ . ....	75
Fig. 4.40.	Magnitude of $y$ -component of electric field internal to a finite circular chiral cylinder along the $z$ -axis, $k_o a = 1.5$ , $h = 0.35\lambda_o$ , $\epsilon_r = 2$ , $\mu_r = 1$ , $\xi_r = 0.0, 0.1, \dots, 0.9$ . ....	76
Fig. 4.41.	Phase of $y$ -component of electric field internal to a finite circular chiral cylinder along the $z$ -axis, $k_o a = 1.5$ , $h = 0.35\lambda_o$ , $\epsilon_r = 2$ , $\mu_r = 1$ , $\xi_r = 0.1, \dots, 0.9$ . ....	76
Fig. 4.42.	Length $l$ along the perimeter of the cross section of a finite circular cylinder in the $\phi = 0$ plane. ....	77
Fig. 4.43.	Magnitude of $t$ -component of magnetic current in the $\phi = 0$ plane of a finite circular chiral cylinder, $k_o a = 1.5$ , $h = 0.35\lambda_o$ , $\epsilon_r = 2$ , $\mu_r = 1$ , $\xi_r = 0.0, 0.4$ , and $0.8$ . ....	78

Fig. 4.44.	Phase of $t$ -component of magnetic current in the $\phi = 0$ plane of a finite circular chiral cylinder, $k_o a = 1.5$ , $h = 0.35\lambda_o$ , $\epsilon_r = 2$ , $\mu_r = 1$ , $\xi_r = 0.0, 0.4$ , and $0.8$ . . . . .	78
Fig. 4.45.	Magnitude of $l$ -component of magnetic current in the $\phi = 0$ plane of a finite circular chiral cylinder, $k_o a = 1.5$ , $h = 0.35\lambda_o$ , $\epsilon_r = 2$ , $\mu_r = 1$ , $\xi_r = 0.0, 0.4$ , and $0.8$ . . . . .	79
Fig. 4.46.	Phase of $l$ -component of magnetic current in the $\phi = 0$ plane of a finite circular chiral cylinder, $k_o a = 1.5$ , $h = 0.35\lambda_o$ , $\epsilon_r = 2$ , $\mu_r = 1$ , $\xi_r = 0.4$ and $0.8$ . . . . .	79
Fig. 4.47.	Magnitude of $t$ -component of electric current in the $\phi = 0$ plane of a finite circular chiral cylinder, $k_o a = 1.5$ , $h = 0.35\lambda_o$ , $\epsilon_r = 2$ , $\mu_r = 1$ , $\xi_r = 0.0, 0.4$ , and $0.8$ . . . . .	80
Fig. 4.48.	Phase of $t$ -component of electric current in the $\phi = 0$ plane of a finite circular chiral cylinder, $k_o a = 1.5$ , $h = 0.35\lambda_o$ , $\epsilon_r = 2$ , $\mu_r = 1$ , $\xi_r = 0.4$ and $0.8$ . . . . .	80
Fig. 4.49.	Magnitude of $l$ -component of electric current in the $\phi = 0$ plane of a finite circular chiral cylinder, $k_o a = 1.5$ , $h = 0.35\lambda_o$ , $\epsilon_r = 2$ , $\mu_r = 1$ , $\xi_r = 0.0, 0.4$ , and $0.8$ . . . . .	81
Fig. 4.50.	Phase of $l$ -component of electric current in the $\phi = 0$ plane of a finite circular chiral cylinder, $k_o a = 1.5$ , $h = 0.35\lambda_o$ , $\epsilon_r = 2$ , $\mu_r = 1$ , $\xi_r = 0.0, 0.4$ , and $0.8$ . . . . .	81
Fig. 4.51.	Convergence of $ E_x/E^{\text{inc}} $ at $(x, y, z) = (0, 0, 0.4d)$ for a chiral cube, $d = 0.35\lambda_o$ , $\epsilon_r = 2$ , $\mu_r = 1$ , $\xi_r = 0.0, 0.1, \dots, 0.9$ . . . . .	83
Fig. 4.52.	Estimated percent error of $ E_x $ at $(x, y, z) = (0, 0, 0.4d)$ for a chiral cube, $d = 0.35\lambda_o$ , $\epsilon_r = 2$ , $\mu_r = 1$ , $\xi_r = 0.0, 0.1, \dots, 0.9$ . Solid lines are computed by the approximating function. . . . .	83
Fig. 4.53.	$\sigma_{\text{ee}}$ of a chiral cube, $d = 0.35\lambda_o$ , $\epsilon_r = 2$ , $\mu_r = 1$ , $\xi_r = 0.0, 0.1, \dots, 0.9$ . . . . .	86

Fig. 4.54.	$\sigma_{\infty}$ of a chiral cube, $d = 0.35\lambda_o$ , $\epsilon_r = 2$ , $\mu_r = 1$ , $\xi_r = 0.0, 0.1, \dots, 0.9$ . . . . .	87
Fig. 4.55.	$\sigma_{\infty}$ of a chiral cube, $d = 0.35\lambda_o$ , $\epsilon_r = 2$ , $\mu_r = 1$ , at $\theta = 0^\circ, 45^\circ, 90^\circ, 135^\circ, 180^\circ$ . . . . .	88
Fig. 4.56.	$\sigma_{\infty}$ of a chiral cube, $d = 0.35\lambda_o$ , $\epsilon_r = 2$ , $\mu_r = 1$ , at $\theta = 0^\circ, 45^\circ, 90^\circ, 135^\circ, 180^\circ$ . . . . .	88
Fig. 4.57.	Magnitude of $x$ -component of electric field internal to a chiral cube along the $z$ -axis, $d = 0.35\lambda_o$ , $\epsilon_r = 2$ , $\mu_r = 1$ , $\xi_r = 0.0, 0.3, 0.4, \dots, 0.9$ . . . . .	89
Fig. 4.58.	Phase of $x$ -component of electric field internal to a chiral cube along the $z$ -axis, $d = 0.35\lambda_o$ , $\epsilon_r = 2$ , $\mu_r = 1$ , $\xi_r = 0.0, 0.3, 0.4, \dots, 0.9$ . . .	89
Fig. 4.59.	Magnitude of $y$ -component of electric field internal to a chiral cube along the $z$ -axis, $d = 0.35\lambda_o$ , $\epsilon_r = 2$ , $\mu_r = 1$ , $\xi_r = 0.0, 0.1, \dots, 0.9$ . .	90
Fig. 4.60.	Phase of $y$ -component of electric field internal to a chiral cube along the $z$ -axis, $d = 0.35\lambda_o$ , $\epsilon_r = 2$ , $\mu_r = 1$ , $\xi_r = 0.1, \dots, 0.9$ . . . . .	90
Fig. 4.61.	Length $l$ along the perimeter of the cross section of a cube in the $\phi = 0$ plane. . . . .	91
Fig. 4.62.	Magnitude of $t$ -component of magnetic current in the $\phi = 0$ plane of a chiral cube, $d = 0.35\lambda_o$ , $\epsilon_r = 2$ , $\mu_r = 1$ , $\xi_r = 0.0, 0.4$ , and $0.8$ . . .	92
Fig. 4.63.	Phase of $t$ -component of magnetic current in the $\phi = 0$ plane of a chiral cube, $d = 0.35\lambda_o$ , $\epsilon_r = 2$ , $\mu_r = 1$ , $\xi_r = 0.0, 0.4$ , and $0.8$ . . . . .	92
Fig. 4.64.	Magnitude of $l$ -component of magnetic current in the $\phi = 0$ plane of a chiral cube, $d = 0.35\lambda_o$ , $\epsilon_r = 2$ , $\mu_r = 1$ , $\xi_r = 0.0, 0.4$ , and $0.8$ . . .	93
Fig. 4.65.	Phase of $l$ -component of magnetic current in the $\phi = 0$ plane of a chiral cube, $d = 0.35\lambda_o$ , $\epsilon_r = 2$ , $\mu_r = 1$ , $\xi_r = 0.4$ and $0.8$ . . . . .	93
Fig. 4.66.	Magnitude of $t$ -component of electric current in the $\phi = 0$ plane of a chiral cube, $d = 0.35\lambda_o$ , $\epsilon_r = 2$ , $\mu_r = 1$ , $\xi_r = 0.0, 0.4$ , and $0.8$ . . . . .	94



Fig. 4.67.	Phase of $t$ -component of electric current in the $\phi = 0$ plane of a chiral cube, $d = 0.35\lambda_o$ , $\epsilon_r = 2$ , $\mu_r = 1$ , $\xi_r = 0.4$ and $0.8$ . . . . .	94
Fig. 4.68.	Magnitude of $l$ -component of electric current in the $\phi = 0$ plane of a chiral cube, $d = 0.35\lambda_o$ , $\epsilon_r = 2$ , $\mu_r = 1$ , $\xi_r = 0.0, 0.4$ , and $0.8$ . . . . .	95
Fig. 4.69.	Phase of $l$ -component of electric current in the $\phi = 0$ plane of a chiral cube, $d = 0.35\lambda_o$ , $\epsilon_r = 2$ , $\mu_r = 1$ , $\xi_r = 0.0, 0.4$ , and $0.8$ . . . . .	95
Fig. 4.70.	Real parts of $\mathbf{J}/ H^{\text{inc}} $ and $\mathbf{M}/ E^{\text{inc}} $ in the $\phi = 0$ plane of a chiral cube, $d = 0.35\lambda_o$ , $\epsilon_r = 2$ , $\mu_r = 1$ , $\xi_r = 0.0$ . . . . .	98
Fig. 4.71.	Imaginary parts of $\mathbf{J}/ H^{\text{inc}} $ and $\mathbf{M}/ E^{\text{inc}} $ in the $\phi = 0$ plane of a chiral cube, $d = 0.35\lambda_o$ , $\epsilon_r = 2$ , $\mu_r = 1$ , $\xi_r = 0.0$ . . . . .	98
Fig. 4.72.	Real part of $\mathbf{M}_x/ E^{\text{inc}} $ in the $\phi = 0$ plane of a chiral cube, $d = 0.35\lambda_o$ , $\epsilon_r = 2$ , $\mu_r = 1$ , $\xi_r = 0.0$ . . . . .	99
Fig. 4.73.	Imaginary part of $\mathbf{M}_x/ E^{\text{inc}} $ in the $\phi = 0$ plane of a chiral cube, $d = 0.35\lambda_o$ , $\epsilon_r = 2$ , $\mu_r = 1$ , $\xi_r = 0.0$ . . . . .	99
Fig. 4.74.	Real parts of $\mathbf{J}/ H^{\text{inc}} $ and $\mathbf{M}/ E^{\text{inc}} $ in the $\phi = 0$ plane of a chiral cube, $d = 0.35\lambda_o$ , $\epsilon_r = 2$ , $\mu_r = 1$ , $\xi_r = 0.9$ . . . . .	100
Fig. 4.75.	Imaginary parts of $\mathbf{J}/ H^{\text{inc}} $ and $\mathbf{M}/ E^{\text{inc}} $ in the $\phi = 0$ plane of a chiral cube, $d = 0.35\lambda_o$ , $\epsilon_r = 2$ , $\mu_r = 1$ , $\xi_r = 0.9$ . . . . .	100
Fig. 4.76.	Real part of $\mathbf{M}_x/ E^{\text{inc}} $ in the $\phi = 0$ plane of a chiral cube, $d = 0.35\lambda_o$ , $\epsilon_r = 2$ , $\mu_r = 1$ , $\xi_r = 0.9$ . . . . .	101
Fig. 4.77.	Imaginary part of $\mathbf{M}_x/ E^{\text{inc}} $ in the $\phi = 0$ plane of a chiral cube, $d = 0.35\lambda_o$ , $\epsilon_r = 2$ , $\mu_r = 1$ , $\xi_r = 0.9$ . . . . .	101
Fig. 4.78.	Three of the six faces of a cube when the plane of polarization of the incident wave is the $\phi = \phi^{\text{inc}}$ plane. . . . .	103

Fig. 4.79.	Cross-polarized backscattering cross section of a chiral cube, $d = 0.35\lambda_0$ , $\epsilon_r = 2$ , $\mu_r = 1$ , $\xi_r = 0.0, 0.1, \dots, 0.9$ with $0^\circ \leq \phi^{\text{inc}} \leq 90^\circ$ .....	104
Fig. 4.80.	Plane views of an ellipsoid, no 90-degree rotational symmetry. ....	106
Fig. 4.81.	Plane views of an elliptical finite cylinder, no 90-degree rotational symmetry. ....	107
Fig. 4.82.	Plane views of a rectangular parallelepiped, no 90-degree rotational symmetry. ....	108
Fig. 4.83.	Plane views of a right parallelepiped, no 90-degree rotational symmetry. ....	109
Fig. A.1.	$\sigma_{\theta\theta}$ of a chiral sphere, $\epsilon_r = 4$ , $\mu_r = 1$ , $\xi_r = 0, 0.1, 0.3, 0.5$ . ....	135
Fig. A.2.	$\sigma_{\phi\phi}$ of a chiral sphere, $\epsilon_r = 4$ , $\mu_r = 1$ , $\xi_r = 0, 0.1, 0.3, 0.5$ . ....	135
Fig. A.3.	$\sigma_{\theta\theta}$ of a chiral sphere, $\epsilon_r = \frac{4}{1-\xi_r^2}$ , $\mu_r = \frac{1}{1-\xi_r^2}$ , $\xi_r = 0, 0.1, 0.3, 0.5$ . ..	136
Fig. A.4.	$\sigma_{\phi\phi}$ of a chiral sphere, $\epsilon_r = \frac{4}{1-\xi_r^2}$ , $\mu_r = \frac{1}{1-\xi_r^2}$ , $\xi_r = 0, 0.1, 0.3, 0.5$ . ..	136
Fig. A.5.	$x$ for $\epsilon_r = 10$ , $\mu_r = 1$ , and $n=1$ .....	145
Fig. A.6.	$y$ for $\epsilon_r = 10$ , $\mu_r = 1$ , and $n=1$ .....	146
Fig. A.7.	$Q$ for $\epsilon_r = 10$ , $\mu_r = 1$ , and $n=1$ .....	146
Fig. B.1.	Surface where current $\mathbf{J}(\mathbf{M})$ resides. ....	156
Fig. B.2.	Surface $S_0$ located on $xy$ -plane. ....	157
Fig. C.1.	Triangle pair and geometrical parameters associated with the $n^{\text{th}}$ edge. ....	160
Fig. C.2.	Definition of the normalized area coordinates. ....	162
Fig. C.3.	Definition of the variables used in (C-28) and (C-29). ....	166
Fig. D.1.	Definition of the normalized area coordinates. ....	167

## List of Tables

Table 4.1.	Coefficients $A$ and $B$ of the approximating function for the %error of $ E_x $ at $z = 0.795a$ for a chiral sphere, $k_o a = 1.5$ , $\epsilon_r = 2$ , $\mu_r = 1$ .....	48
Table 4.2.	Coefficients $A$ and the estimated values of the exact solution for $ E_x/E^{\text{inc}} $ at $z = 0.4h$ for a finite circular chiral cylinder, $k_o a = 1.5$ , $h = 0.35\lambda_o$ , $\epsilon_r = 2$ , $\mu_r = 1$ .....	69
Table 4.3.	Coefficients $A$ and the estimated values of the exact solution for $ E_x/E^{\text{inc}} $ at $z = 0.4d$ for a chiral cube, $d = 0.35\lambda_o$ , $\epsilon_r = 2$ , $\mu_r = 1$ .....	84
Table 4.4.	The numerical results obtained in previous sections of $\sigma_{\theta\theta}$ in the backward direction normalized to $\sigma_{\theta\theta}$ in the forward direction of a chiral sphere, a finite circular chiral cylinder, and a chiral cube when $\epsilon_r = 2$ , $\mu_r = 1$ .....	102
Table 4.5.	The numerical results of $\sigma_{\theta\theta}$ in the backward direction normalized to $\sigma_{\theta\theta}$ in the forward direction of the objects of Figs. 4.80–4.83. ....	105
Table D.1.	Gaussian quadrature rules of degree 10, $NG=25$ .....	168
Table D.2.	Gaussian quadrature rules of degree 16, $NG=52$ .....	169

## **Acknowledgements**

I would like to express my sincere gratitude and appreciation to my advisor, Dr. Ercument Arvas, for his guidance, encouragement and critical review throughout the course of this research.

I would like to express my sincere thanks to Dr. Joseph R. Mautz for his carefully review of this dissertation and his helpful suggestions, which have enhanced this dissertation. I would like to extend my appreciation to Dr. Jay K. Lee, Dr. Philipp Kornreich, Dr. James R. Willhite, and Dr. Thong Q. Dang for serving as members of the oral examination committee.

I would like to thank my colleagues, Samir L. Tozin and Tehsin Douglas Huang, for their useful discussions and their helps in proofreading a part of this dissertation.

I would like to thank my parents and my sisters for their endless love, understanding, encouragement, and support throughout my entire educational career. Finally, I would like to thank Izumi Sakashita for making my life meaningful.

# Chapter 1

## Introduction

In this dissertation, the problem of electromagnetic scattering from a three-dimensional homogeneous chiral body of arbitrary shape is solved numerically using the method of moments. The effect of adding chirality is investigated by numerical results. The main purpose of this research is to compute scattered fields in the far region or the radar cross section (RCS). The numerical solution for scattering is verified by comparing with the analytical result for a chiral sphere [Appendix A].

### 1.1 Chiral Medium

A chiral medium has the property to rotate the plane of polarization of a linearly polarized wave. When a linearly polarized wave is incident normally upon a slab of chiral medium, two waves are generated in the medium. These two waves have opposite handedness and unequal phase velocity. Beyond the slab, the two waves combine to yield a linearly polarized wave whose plane of polarization is rotated with respect to the plane of polarization of the incident wave [1].

The phenomenon of chirality is known in optics as the optical activity phenomenon. An optically active medium has the property to rotate the plane of polarization of linearly polarized light rays. The optical activity phenomenon has been discovered by Arago [2] by observing that a crystal of quartz rotates the plane of polarization of linearly polarized light. Subsequent experiments on plates of quartz have been done by Biot [3–5]. Biot concluded that the optical activity depends on the thickness of the plate and the wavelength of light, and the optical activity is absent when two plates of the same thickness but opposite handedness are put together. Biot [6] also discovered the optical

activity phenomenon in organic liquids such as oils of turpentine and laurel, alcoholic solutions of camphor, and aqueous solutions of sugar and tartaric acid. Pasteur [7] interpreted Biot's observations that the arrangement of atoms within a chiral medium is asymmetric. The optical activity of a medium is caused by the chirality of its molecules.

In 1920, Lindman [8] introduced a new approach to study chirality by using small helices, man-made chiral objects, instead of chiral molecules, and demonstrated the phenomenon of optical activity using microwaves instead of light. Lindman synthesized a chiral medium by twisting small helices from copper wire, immersing these helices in cotton balls, and then positioning the balls with random orientation in a cardboard box. The length of the straight wire of the helices was 9 cm with a diameter of 1.2 mm. The diameter of the spirals was 10 mm and there were 2.5 turns in one helix. The cardboard box was 26 cm long and the total number of spirals was 700. The results proved the existence of polarization rotation and the dispersion of the activity around 1 to 3 GHz. The results also showed that the angle of rotation is directly proportional to the number of helices in the box. Lindman also proved that the mixture of equal amounts of left- and right-handed helices was electromagnetically inactive. Lindman compared his measurements against a model for optical activity in [9]. The work of Lindman is summarized in [10]. Lindman's results have been confirmed by experiments performed by Winkler [11], Tinoco and Freeman [12]. Researches related to the constructions of artificial chiral media at microwave frequency have been reported by [13–15]. The preparation of chiral dielectric slabs that contain right-handed only, left-handed only, and an equal mixture of left- and right-handed miniature helices of various concentrations

with random distributions is described in [16]. The aforementioned researches are solid experimental proofs of the existence of chiral media at microwave frequency.

## 1.2 Constitutive Relations

There are three sets of constitutive relations most commonly used in the literature. The first one has been proposed by Fedorov in 1959 [17]. Fedorov modified Born's proposal for isotropic chiral media [18], which was inspired by the study of Drude [19]. This set of constitutive relations is labeled as the Drude-Born-Fedorov relations. These relations are used by some researchers [20–24]. The Drude-Born-Fedorov relations are defined as

$$\mathbf{D} = \varepsilon_{\text{DBF}} (\mathbf{E} + \xi_{\text{DBF}} \nabla \times \mathbf{E}) \quad (1-1)$$

$$\mathbf{B} = \mu_{\text{DBF}} (\mathbf{H} + \xi_{\text{DBF}} \nabla \times \mathbf{H}). \quad (1-2)$$

The second one was proposed by Post in 1962 [25]. This set of constitutive relations is labeled as the Post relations. These relations are used by some researchers [26–30]. The Post relations are defined as

$$\mathbf{D} = \varepsilon_p \mathbf{E} - j\xi_p \mathbf{B} \quad (1-3)$$

$$\mathbf{H} = \frac{1}{\mu_p} \mathbf{B} - j\xi_p \mathbf{E}. \quad (1-4)$$

The third one is used in this dissertation. These relations are in the book by Lindell [31] and used by some researchers [32–34]. The constitutive relations are defined as

$$\mathbf{D} = \varepsilon \mathbf{E} - j\xi \mathbf{H} \quad (1-5)$$

$$\mathbf{B} = \mu \mathbf{H} + j\xi \mathbf{E}. \quad (1-6)$$

These three sets of constitutive relations are equivalent. The transformations between the parameters of different systems are given by [31, pp. 309–310] as

$$\varepsilon = \varepsilon_p + \mu_p \xi_p^2 = \frac{\varepsilon_{\text{DBF}}}{1 - (k_{\text{DBF}} \xi_{\text{DBF}})^2} \quad (1-7)$$

$$\mu = \mu_p = \frac{\mu_{\text{DBF}}}{1 - (k_{\text{DBF}} \xi_{\text{DBF}})^2} \quad (1-8)$$

$$\xi = \mu_p \xi_p = \frac{k_{\text{DBF}} \xi_{\text{DBF}} \sqrt{\mu_{\text{DBF}} \varepsilon_{\text{DBF}}}}{1 - (k_{\text{DBF}} \xi_{\text{DBF}})^2} \quad (1-9)$$

where

$$k_{\text{DBF}} = \omega \sqrt{\mu_{\text{DBF}} \varepsilon_{\text{DBF}}} . \quad (1-10)$$

In this research the relative chirality,  $\xi_r$ , is defined as follows.

$$\xi_r = \frac{\xi}{\sqrt{\mu \varepsilon}} = \frac{\mu_p \xi_p}{\sqrt{\mu_p (\varepsilon_p + \mu_p \xi_p^2)}} = k_{\text{DBF}} \xi_{\text{DBF}} . \quad (1-11)$$

Lindell [31, pp. 35] shows that a z-traveling linearly polarized plane wave of electric field in a chiral medium can be written as

$$\mathbf{E} = E_0 e^{-jkz} [\mathbf{a}_x \cos(\xi_r kz) - \mathbf{a}_y \sin(\xi_r kz)] \quad (1-12)$$

where

$$k = \omega \sqrt{\mu \varepsilon} . \quad (1-13)$$

The vector in square brackets of (1-12) is a unit vector, which is rotated from the position  $\mathbf{a}_x$  by the angle  $\phi = -\xi_r kz$ . When  $\xi_r$  is positive, the rotation of the plane of polarization of a linearly polarized plane wave is in the left-hand direction (counterclockwise) when looking in the direction of propagation. This chiral medium is called a right-handed medium. When  $\xi_r$  is negative, the rotation of the plane of polarization of a linearly polarized plane wave is in the right-hand direction (clockwise) when looking in the direction of propagation. This chiral medium is called a left-handed medium.